

Cite this: *Phys. Chem. Chem. Phys.*,  
2014, 16, 516

# Time resolved observation of the solvation dynamics of a Rydberg excited molecule deposited on an argon cluster-I: DABCO<sup>☆</sup> at short times<sup>†</sup>

Slim Awali,<sup>a,bc</sup> Lionel Poisson,<sup>\*ab</sup> Benoît Soep,<sup>ab</sup> Marc-André Gaveau,<sup>ab</sup> Marc Briant,<sup>ab</sup> Christophe Pothier,<sup>ab</sup> Jean-Michel Mestdagh,<sup>ab</sup> Mounir Ben El Hadj Rhouma,<sup>c</sup> Majdi Hochlaf,<sup>d</sup> Vincent Mazet<sup>e</sup> and Sylvain Faisan<sup>e</sup>

Received 26th July 2013,  
Accepted 13th September 2013

DOI: 10.1039/c3cp53172d

[www.rsc.org/pccp](http://www.rsc.org/pccp)

This paper is a joint experimental and theoretical approach concerning a molecule deposited on a large argon cluster. The spectroscopy and the dynamics of the deposited molecule are measured using the photoelectron spectroscopy. The absorption spectrum of the deposited molecule shows two solvation sites populated in the ground state. The combined dynamics reveals that the population ratio of the two sites is reversed when the molecule is electronically excited. This work provides the timescale of the corresponding solvation dynamics. Theoretical calculation supports the interpretation. More generally, close examination of the short time dynamics (0–6 ps) of DABCO···Ar<sub>n</sub> gives insights into the ultrafast relaxation dynamics of molecules deposited at interfaces and provides hence the time scale for deposited molecules to adapt to their neighborhoods.

## 1 Introduction

In the condensed phase, solvation perturbs strongly the electronic excited states of molecules, causing a change in the pattern and shape of the electronic states and, therefore, in the reaction dynamics. Indeed these effects can stem from the level shifting under solvation or even the change in the order of the excited states, a classical example being differential solvation of nπ<sup>☆</sup> and ππ<sup>☆</sup> states of organic molecules. Generally solvation effects become dramatic for high lying diffuse states like Rydberg states. Indeed, as observed early for Rydberg states in rare gas matrices, the energy of the Rydberg levels is upshifted<sup>1,2</sup> until abruptly the conduction band is reached at rather low *n*'s.

This stems from the repulsion of the diffuse Rydberg orbitals by the atoms from the matrix, until the Rydberg cloud extends beyond them and they interact with the core ion, thus

deeply solvated.<sup>2–6</sup> Spectroscopy and real-time experiments in matrices have been performed to investigate the influence of condensed media on the Rydberg states.<sup>7–9</sup> This interaction has been characterized in experiments on excited Van der Waals complexes where an excited Rydberg atom, Hg, interacts with rare gases. In these systems, the interaction potential is repulsive at a long distance owing to the exchange interaction between the Rydberg and the rare gas electrons. It switches to be strongly attractive at a short distance when the ion core is no longer screened by the Rydberg electron.<sup>10</sup> Of course, the higher the quantum number, the larger the Rydberg radius (as square of the quantum number) and the larger the latter switch distance.

We investigate here, instead of a perturbing atom, a rare gas cluster. This is a perturbing medium intermediate between an isolated atom and a matrix since the atoms of the cluster are much free to accommodate a foreign atom or a molecule, especially if the Rydberg molecule sits at the surface of the cluster or close to it. Then the interaction between a rare gas cluster and a molecule excited in a Rydberg state comes very close to that described for Hg<sup>☆</sup>···Ar. We examine here the fate of a system, 1,4-diazabicyclo-[2.2.2]octane (DABCO), a compact molecule whose first excited state is of strong Rydberg character (the wave function is 90% Rydberg-3s<sup>11</sup>), deposited on an Ar<sub>n</sub> cluster by following its relaxation dynamics after excitation.<sup>11–13</sup> The ground electronic state of the DABCO molecule is however a valence state in nature. Hence, different solvation effects are expected when the molecule is promoted into the S<sub>1</sub> state. This is

<sup>a</sup> CNRS, IRAMIS, SPAM, Laboratoire Francis Perrin, URA 2453, F-91191 Gif-sur-Yvette, France. E-mail: lionel.poisson@cea.fr

<sup>b</sup> CEA, IRAMIS, SPAM, Laboratoire Francis Perrin, URA 2453, F-91191 Gif-sur-Yvette, France

<sup>c</sup> EMIR, Institut Préparatoire aux Etudes d'Ingénieurs, Monastir, Tunisie

<sup>d</sup> Université Paris-Est, Laboratoire Modélisation et Simulation Multi-Echelle, MSME UMR 8208 CNRS 5 bd Descartes, 77454 Marne-la-Vallée, France

<sup>e</sup> ICube, University of Strasbourg, CNRS, 300 boulevard Sébastien Brant, BP 10413, 67412 Illkirch, France

† Electronic supplementary information (ESI) available. See DOI: 10.1039/c3cp53172d

performed by combining the information from the spectroscopy and the ultrafast dynamics for a full interpretation and characterization of this process. For this purpose, the DABCO molecule<sup>14</sup> is especially interesting and well suited. It has been extensively studied<sup>15–17</sup> because of the Rydberg character of its S<sub>1</sub> state due to the strain of its geometry and to its low Ionization Energy (IE).<sup>18,19</sup>

Furthermore, it presents only one low energy mode<sup>20–22</sup> which is the strongly anharmonic torsional mode. Calculations on the isolated molecule have also been performed.<sup>17,23</sup> The interaction with various solvents, among them argon clusters, has been spectroscopically investigated quite extensively as well as theoretically.<sup>24–26</sup>

It is worth noticing that the spectroscopic shift for the S<sub>1</sub> state, from DABCO to DABCO··Ar<sub>3</sub>, is increasing regularly by  $\approx 100\text{ cm}^{-1}$  for each argon atom.<sup>25</sup> Micro-second dynamics of the solvated molecule were also performed and showed a 1.8  $\mu\text{s}$  fluorescence decay for the isolated molecule and 1.7 or 1.4  $\mu\text{s}$  for DABCO··Ar depending on the relative location of the argon atoms around the DABCO molecule.<sup>27</sup> This time reduction was interpreted in terms of solvent induced intersystem crossing to the triplet state. Recently, Mathivon *et al.*<sup>28,29</sup> reinvestigated the neutral and ionic DABCO··Ar<sub>n</sub> (small *n*) heteroclusters by means of modern theoretical methodologies. They characterized the stationary points on the ground state potential energy surfaces and they mapped the evolution of their electronic excited states. Mainly, they showed that the cluster electronic states present also a Rydberg character, as the bare molecule and that the wavepacket dynamics on these potentials may be complex.

## 2 Experimental section

The present paper focuses on the DABCO molecule deposited on an argon cluster. This system was studied on two experimental setups, the first one being devoted to the spectroscopy of van-der-Waals clusters in the visible and UV range (Nano),<sup>30</sup> and the second one being devoted to the time-resolved femtochemistry (Femto).<sup>31–33</sup> In the following, we will describe the experimental setups and characterize the cluster beam.

### 2.1 Experimental setups

In both experiments a cluster generation source was coupled with a pick-up deposition cell<sup>34</sup> (Fig. 1). The argon cluster beam is generated by a pulse valve (Parker-Hannifin) coupled to a 100  $\mu\text{m}$  nozzle. A backing pressure of 16 bar is used for the experiment and the corresponding average cluster size is estimated to be around Ar<sub>800</sub>.<sup>32</sup> A series of 2 skimmers is aligned in the same chamber. In-between are located two needles (diameter  $\varnothing 1\text{ mm}$ ) aligned with the cluster beam and connected to a gas line. The molecule of interest is introduced in a flask previously degassed. The temperature of the flask is maintained at the laser-room temperature (21 °C). The vapor flowing to the needle is controlled by a micro leak and measured by a thermalized capacitive gauge in a compression chamber. The whole source is located in the same

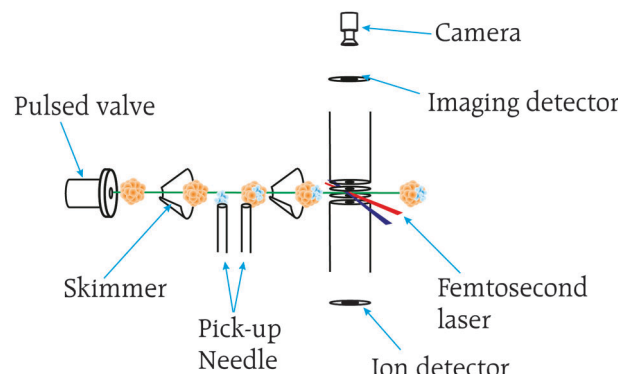


Fig. 1 Experimental setup.

chamber which is coupled to two magnetic turbomolecular pumps giving a total pumping rate of 3900 l s<sup>-1</sup> for a 20 Hz Femto experiment and a single turbomolecular pumping rate of 2200 l s<sup>-1</sup> for the 10 Hz Nano experiment. The first skimmer is attached to a 11 cm diameter flange that lets the pressure between the two skimmers low enough during the traveling time of the clusters to avoid beam destruction. Through the second skimmer, the beam reaches the main chamber that is pumped by both a turbomolecular pump (1600 l s<sup>-1</sup>) and a cryopump.

In the experiment devoted to spectroscopy, the system of study is ionized *via* a resonant two photon excitation using a lambda Physik FL 3000 Nd:YAG pumped dye laser with a resolution of 0.1 cm<sup>-1</sup> at 260 nm. It is used in the domain of the rhodamine 6G dye in ethanol. Photoelectrons are collected as a function of the wavelength in order to get a complete (Resonance Enhanced MultiPhoton Ionization-PhotoElectron Spectroscopy) REMPI-PES characterization. In the present Velocity Map Imaging (VMI) device<sup>35</sup> the electrodes can be rotated by 90° to operate the ionisation in a standard Wiley-MacLaren mode allowing for maximum mass resolution for high masses. In the present study, only the photoelectron device was used. The energy calibration was performed using a potassium source ionized using a REMPI Scheme on its 4p electronics levels:  $E\text{ (eV)} = (8.65 \pm 0.1) \times r^2 \times 10^{-5}$ , where *r* is the distance from the center of the image expressed in pixel.

In the experiment devoted to time resolved photoelectron spectroscopy (fs-TRPES),<sup>36</sup> the deposited system is probed using a femtosecond laser (LUCA part of the SLIC European facility).<sup>17</sup> The fundamental laser wavelength was measured to be between 789 and 792 nm (fwhm 22 nm). Second and third harmonics were obtained by doubling and mixing in BBO Crystals. The second harmonic was measured around 399–400 nm and the third was measured between 265.1 and 266.3 nm. The measurement of the wavelength is usually done for each experiment. Ions and electrons are extracted orthogonally. Ions are detected by means of a Time-of-Flight spectrometer mounted opposite to the VMI. Both speed distributions of ions and electrons can be monitored using a VMI<sup>35</sup> device. This last detection method is well adapted for low intensity signals, since it enables a full 4π solid angle charged species collection and since ions and electrons do not cross any meshes

before reaching the detector. The main drawback of both spectrometers is the non-detection of heavy mass species ( $\text{Ar}_{800}\cdots\text{DABCO}^+ \sim 32 \text{ kg mol}^{-1}$ ), which cannot even reach the detectors. The energy calibration has been performed by irradiation of  $\text{O}_2$  molecules by the third harmonics of the laser that shows a vibrational progression.<sup>37</sup> It can be assigned and accurately fitted for various repeller values and various extractor/repeller ratios. The calibration used in the present paper is also  $E \text{ (eV)} = (1.52 \times (\text{Ext}/\text{Rep} - 0.51) \times (\text{Rep} + 77.0) \pm 2\%) \times r^2 \times 10^{-7}$ .

After detection, the energy profile and ejection angles of the ions or electrons are reconstructed from the raw data using a pBASEX algorithm<sup>38,39</sup> based on the inverse Abel transform. Low energy ions and electrons are especially well-resolved using this technique.

## 2.2 Beam characterization

Focussing the first harmonic of the fs Ti:Sapphire on the argon cluster beam induces the ionization of both isolated argon atoms and argon clusters.<sup>32</sup> The pulsed argon cluster beam is also characterized by monitoring the velocity map distribution of the ion mass distribution as a function of time delay between the pulse valve and the focused pulsed laser (see Fig. 2). By mass selecting the argon atoms, we have access to the argon velocity distribution, which provides information on the beam translational temperature. Whereas by gating the detector to get rid of the argon mass, the cluster distribution becomes accessible. The cluster size distribution after ionization is directly observed on the image for the small cluster size distribution, at the beginning and at the end of the cluster gas pulse. As seen earlier, the detection efficiency of argon clusters is decreasing as their mass increases. In the core of the

gas pulse, the intensity and the size of the argon cluster distribution can be estimated from the signal issued from the coulombic explosion of the cluster.<sup>32</sup>

By defocussing the pump and probe laser ( $\sim 4\text{--}5 \text{ cm}$  from the focus point), argon atoms and clusters are not ionized and become transparent to photons. When turning on the pick-up, the molecules and their clusters are then the only compounds subject to ionization. The pulsed cluster beam is then monitored by investigating the photoelectron signal as a function of the delay between the pulse valve and the laser pulse. Under these conditions, and by comparison with the study under focused laser conditions providing the time delayed density profile of the argon beam, the deposition of the molecule is monitored.

Some deposited molecules on clusters can be ejected from the cluster during the ionization process. They are also detected at their corresponding mass. This depends strongly on the molecule considered and especially on the ionization process in action: after a direct ionization, the molecule is expected to remain reasonably cooled. Whereas, this is not the case after the interaction with laser followed by autoionization. The latter process favors also the ejection.

In the present experiments, we did not observe the ejection of  $\text{DABCO}^+$  ions. Instead, we detected  $\text{Ar}_n\cdots\text{DABCO}^+$  clusters at the rising and falling edge of the cluster signal. The main photoelectron signal is recorded in between. The pulse valve time is adjusted to the maximum of the signal. In addition, the fragmentation of the deposited molecules should be limited even if it can occur on the bare molecule under the same conditions owing to the rapid cooling on the cluster of the excess energy deposited by the probe photons. Nevertheless, all ejected photoelectrons from the clusters are detected. Since the molecules are cooled down by the cluster and remain mostly unfragmented, this photoelectron signal yields an instantaneous snapshot of the cluster at the time it is ionised; it thus provides rich information on the dynamics and spectroscopy of the system. Compared to the usual experiments performed on free molecules,<sup>31,40</sup> the detection of ions from a seeded cluster is not expected to give more information than the photoelectron signal except in the case of an ejection occurring in the probed excited state.<sup>13</sup>

## 2.3 Deposition control

The quantity of DABCO deposited on the argon clusters is controlled by a leak valve. The maximal flux available is limited by the DABCO vapor pressure at room temperature. The CICR method<sup>34</sup> is used to control the average number of DABCO molecules deposited. The photoelectron signal obtained by 2 photon ( $\sim 266 \text{ nm}$ ) ionization of the deposited DABCO is monitored *vs.* the vapor pressure flux. As expected for a first order Poisson distribution with an average number of deposited molecule per cluster  $< 1$ , the photoelectron signal rises linearly with the flux (see Fig. 3). Furthermore, at the maximal flux given by the DABCO vapor pressure at room temperature, only one band is measured, indicating that the average number of DABCO per cluster remains below 1 whatever the gas flux used.

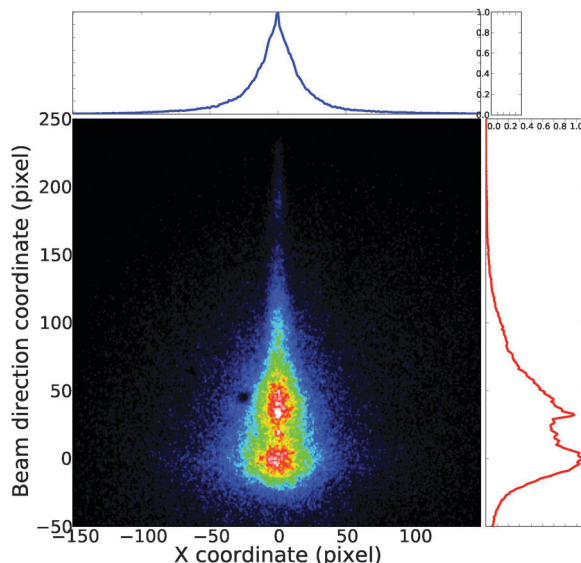


Fig. 2 Raw photoion image collected at the beginning of the cluster pulse under laser focused conditions (800 nm). The curves are the projection of the image along the axes. The detector is gated to remove all masses below 60 a.m.u. For  $(x = 0, y = 33)$  the  $\text{Ar}_2^+$  ion is observed as little spot on the image, which is visible on the right curve as a peak.

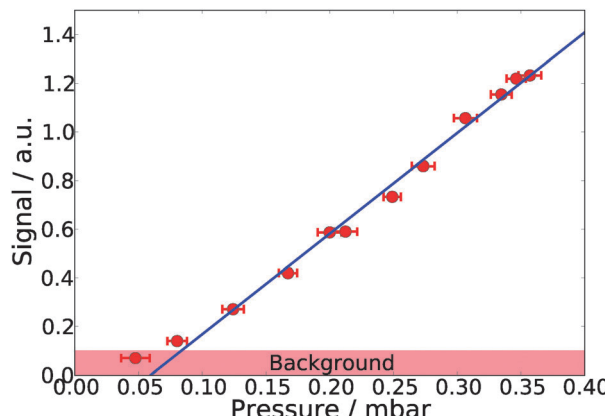


Fig. 3 Evolution of the deposited DABCO photoelectron signal as a function of the DABCO pressure measured in the compression chamber for a back pressure for the generation of the Ar cluster of 16 bar.

### 3 Analysis using the track signal decomposition method

Time resolved dynamics of a deposited molecular system on a rare gas cluster provides a complex signal, which is not possible to fully analyse in time and in photoelectron energy using our standard procedure<sup>11</sup> nor the standard chemometric procedures.<sup>41</sup> Therefore we use a statistical signal processing approach.<sup>42,43</sup> Each spectrum is modeled as the sum of Gaussian peaks and an added noise (the physical justifications of this model can be found in ref. 13 and 44). The signal processing algorithm aims at decomposing each spectrum (each time steps) of the sequence that is to estimate the number of peaks and their parameters (energies, intensities and full width at half maximum (fwhm)) and to follow them through the sequence. A sequential approach, in which the spectra are decomposed independently of the others, is unsuitable.<sup>45</sup> Indeed, the decomposition of two contiguous spectra may lead to two very different decompositions which is physically impossible because the peaks evolve smoothly with time. In contrast, a joint decomposition approach, where spectra are decomposed simultaneously, may favor a smooth change in the peak parameters by regularizing their evolution, thus providing coherent and consistent results. Basically, the joint decomposition approach is set within a Bayesian framework where a Markovian prior favors smooth evolutions of the peaks. In addition, the number of peaks and tracks is unknown and has to be estimated. Thus, the posterior distribution describing the mathematical model is sampled with the reversible jump Markov chain Monte Carlo algorithm.<sup>46</sup> Finally, the estimated decomposition best explains the data with the smallest peak number possible, while favoring tracks with a smooth evolution of their peaks. However, the usual algorithm<sup>42,43</sup> cannot process simultaneously several sequences of spectra, so the P<sub>0</sub>, P<sub>2</sub> and P<sub>4</sub> signals are analysed independently and the solution cannot take into account the specificities of the physics of the relaxation dynamics. Firstly, the decomposition was performed on the P<sub>4</sub> signal which has the lowest number of tracks. Then, the estimated tracks were introduced as a basis for

the P<sub>0</sub> signal, fixing the energy of the peak, while the amplitude and the fwhm are re-estimated in addition to the possibility to include new tracks. Since it appeared that one of the tracks was not properly fitted by a Gaussian function, we introduced a second parallel sub-track at a fixed energy separation ( $-0.033$  eV). Finally, the ensemble of tracks obtained was applied to the three evolutions. Due to the random aspect of the algorithm and to the setting of parameters, different kinds of results can be obtained. We select amongst a set of results, a decomposition having the “best” physical meaning. However a careful analysis of the results is still required, taking into account the assumptions introduced in the model. Some values of parameters obtained may also not be commented.

### 4 Solvated molecule: theoretical aspects

The solvation of the DABCO molecule by argon atoms is examined here using quantum chemistry methods. Since the binding energies between Ar–Ar (of  $\approx 99.2$  cm<sup>-1</sup> ref. 47 and 48) and between DABCO–Ar (of  $\approx 300$  cm<sup>-1</sup>)<sup>28</sup> are of the same order of magnitude, the configuration of Ar atoms around the DABCO molecule is not obvious. Two configurations are possible: (i) the Ar atoms prefer to bind to each other, which leads to a DABCO molecule solvated at the surface of the Ar cluster. (ii) the Ar atoms prefer to bind to DABCO in equivalent positions, which results into a DABCO molecule inside the little rare gas cluster.

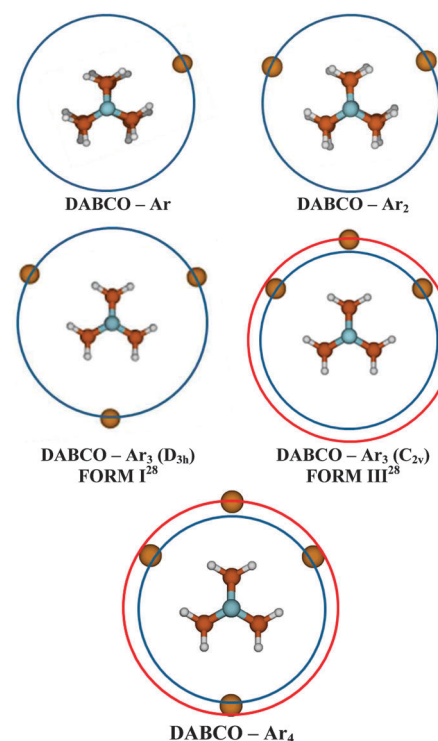


Fig. 4 The most stable forms of DABCO···Ar<sub>n≤4</sub> deduced from ref. 28 and 29. The blue circle corresponds to the first shell of solvation and the red circle to the “second” shell.

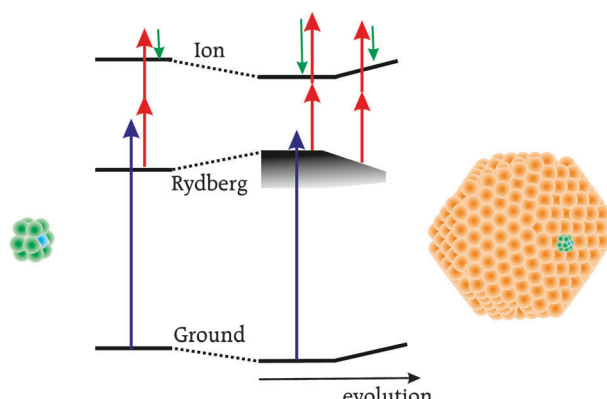


Fig. 5 Schematic presentation of the electronic state changes upon solvation by the argon cluster. The molecule is represented on 800 atom argon clusters.

Recently, Mathivon *et al.*<sup>29</sup> have calculated the optimized geometries of DABCO $\cdots\text{Ar}_{n\leq 4}$  heteroclusters (*cf.* Fig. 4). These calculations are based on modern *ab initio* computations of the minima and the transition states located on the ground potential energy surfaces of neutral and ionic DABCO $\cdots\text{Ar}_{1,2,3,4}$  heteroclusters. Their computed structures are more realistic than previous ones derived either from simple models or from low computation levels.<sup>24,25,49</sup> Hence, Mathivon *et al.*'s findings may be used for getting insights into the location of DABCO within the Ar cluster in the present experimental study. Especially, these recent theoretical computations show that no argon atom binds to nitrogen (transition state configuration regardless of the number of argons). Nevertheless, the energy of this configuration lying below the dissociation energy (200 cm<sup>-1</sup> ref. 28) makes it a situation to consider.

In addition, Mathivon *et al.* investigated the electronic excited states of DABCO $\cdots\text{Ar}_{1,2,3}$ ,<sup>29</sup> which are found to be Rydberg in nature as for the bare molecule. They showed that the parts of the potentials of S<sub>1</sub> of DABCO $\cdots\text{Ar}_3$  FORM I (of D<sub>3h</sub> symmetry) presents a shallow potential well in the Franck-Condon region accessed after vertical excitation from the corresponding ground state. Whereas DABCO $\cdots\text{Ar}_3$  FORM III (of C<sub>2v</sub> symmetry) S<sub>1</sub> potential is repulsive. For all DABCO $\cdots\text{Ar}_{1,2,3}$  species, the S<sub>2</sub> potential presents a slight stabilisation and S<sub>3</sub> and S<sub>4</sub> states are repulsive. In the present experiment, the pump photon energy allows promoting the wavepacket into S<sub>1</sub> and is not sufficient to reach the upper singlets. Owing to the modestly repulsive character of the S<sub>1</sub> surface, the wavepacket generated on this surface will be put into motion on the S<sub>1</sub> potential energy surface before ionisation. This may be generalised to a greater number of argon atoms to picture the evolution of the neutral (ground and Rydberg) and ionic electronic state changes upon DABCO solvation by argon as in Fig. 5. Hence, the ground state is stabilized by dispersion interaction, the ionic state by charge-induced dipole interaction. The Rydberg state, which is larger in size is destabilized at the geometry of the ground state. Its excitation is followed by a dynamics willing for its stabilization.

## 5 Deposited molecule: spectroscopy

### 5.1 Two photon ionization

The experimental procedures we used in the nanosecond spectroscopy experiment and in the time-resolved experiment are very similar: a first laser excites the molecule whereas a second laser ionizes the electronically excited molecule. The difference between the two experiments is the laser pulse duration and the delay between both lasers.

In the case of resonant single color photoionization by femtosecond laser, no solvation dynamics is expected within the pulse duration time ( $\approx 80$  fs). The photoelectron energy is also close to the signal expected from a single photon ionization. The energy difference measured with the isolated molecule is the solvation energy difference taking place between the ion and the ground state for this last geometry.

In the case of nanosecond spectroscopy, the second photon which ionizes the excited molecule comes  $\approx 1$  ns after the first laser which excites the molecule. The excited molecule has enough time to relax its solvation geometry and the photoelectron energy documents also this relaxation.

### 5.2 REMPI-PES spectra

The action spectrum of the deposited DABCO molecule was measured by REMPI over the range 275–265 nm by steps of 0.025 nm. Photoelectron spectra were collected for each wavelength (see Fig. 6). Several photoelectron bands are observed, corresponding to either different species, different excited states or different ionic states.

In Fig. 6, one can identify the photoelectron signal of the isolated DABCO molecule peaking at 2 eV<sup>17</sup> (Peak 3). The evolution of the intensity of this band along the photon energy gives its characteristic REMPI absorption spectrum. When looking at the velocity distribution of the ions, the DABCO<sup>+</sup> ion does not show any orthogonal velocity to the molecular beam, pointing out the absence of ejected molecules after excitation, on the whole wavelength range investigated here.

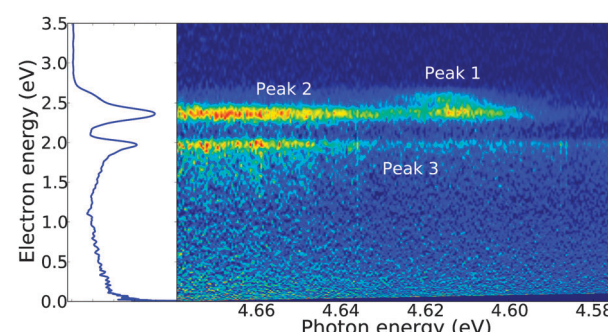
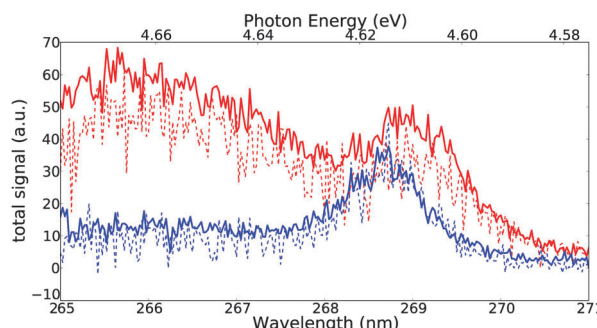


Fig. 6 Photoelectron signal versus the excitation energy in a single photon REMPI experiment. The first photon excites the molecule whereas the second one ionizes it. Since the same photon energy is used for both processes, the photoelectron energy moves as the excitation wavelength changes. The photoelectron spectra have been compensated for the probe energy increase with a linear correction. On the left: projection of the photoelectron spectrum along all wavelengths. The photoelectron energy is the one expected for an experiment at 4.679 eV (265 nm).

**Table 1** The anisotropy parameters are average values evaluated over the full signal range

	Energy (eV)	Energy below IE (eV)	fw hm (eV)	$\beta_2$	$\beta_4$
Peak 1	2.56	-2.12	0.12	[268.5–269 nm] 1.0 ± 0.1 [265–268.5 nm] 0.8 ± 0.1	0.2 ± 0.1 0.0 ± 0.1
Peak 2	2.35	-2.33	0.11	0.8 ± 0.1	0.1 ± 0.1
Peak 3	1.96	-2.72	0.14	1.1 ± 0.1	0.0 ± 0.1

<sup>a</sup> Photoelectron energies for a photon wavelength of 265 nm (4.679 eV).



**Fig. 7** REMPI signal collected on the two DABCO–Ar<sub>n</sub> photoelectron peaks. Continuous line: whole signal. Dashed lines: the P<sub>2</sub> component of the signal. (blue) Peak 1 (red) Peak 2. See Table 1.

The photoelectron signal from DABCO at 2 eV is also not relevant for the present study since it is coming from isolated molecule in the background gas and partially in the beam. Two other photoelectron bands are observed, corresponding to the DABCO molecule deposited on the cluster (see Table 1).

The spectra of Peaks 1 and 2 are presented in Fig. 7. They exhibit definitely very different behaviours. The intensity of photoelectron Peak 2 (photoelectron energy at 2.35 eV) starts to rise for a photon energy of ≈4.585 eV. Two main features are observed: a broad distribution peaking at ≈4.610 eV, followed by a minimum at 4.623 eV, then a wide rising band. The intensity of photoelectron Peak 1 (photoelectron at 2.56 eV) starts to rise at ≈4.592 eV (+7 meV from Peak 1, ≈60 cm<sup>-1</sup>) to generate a broad distribution peaking at ≈4.615 eV (+23 meV, 185 cm<sup>-1</sup> from the rising threshold). The signal depletes at higher photon energies to reach a low level plateau from ≈4.632 eV (+40 meV, 320 cm<sup>-1</sup> from the rising threshold).

The correlated evolution of the P<sub>2</sub> polarized part of the image is represented as dashed lines. Roughly it shows a similar polarization for both bands, with a tiny difference in the range 268–269 nm.

Since no excited states appear to be reachable by the excitation at 265–266 nm,<sup>29</sup> nor some specific vibrational transition in the cluster, the appearance of Peaks 1 and 2 has to be sought within the solvation process. Both the shift in photon energy of ≈60 cm<sup>-1</sup> and the 0.21 eV difference in the ionization potential suggest two different solvation sites for the two photoelectron bands. The one giving the highest photoelectron energy and the highest absorption threshold should correspond to the highest number of argon atoms interacting with

the DABCO molecule. This stems from the experimental results of Shang *et al.*<sup>25</sup> showing a destabilization of S<sub>1</sub> by argon atoms confirmed in the calculations of Mathivon *et al.*<sup>29</sup> Note that the surface of the argon cluster is described to be fluxional, even at 34 K (*i.e.* temperature of this cluster). Hence, the DABCO molecule is most likely in equilibrium between both sites in the ground electronic state. We have shown the existence of two different equilibrium conformations, isomers of DABCO with respect of the argon surface in the S<sub>1</sub> state. This is not surprising in the case of such a large argon cluster.<sup>50</sup> We make the supplementary hypothesis that similar conformations exist in the ground S<sub>0</sub> state, otherwise by optical excitation they would not be accessible separately.

## 6 Deposited molecule: dynamics

### 6.1 Vertical ionization energy

Fig. 8 shows the photoelectron spectra collected with the third harmonic of the femtosecond laser on an argon cluster with DABCO (photons of 4.677 eV). The photoelectron energy measured for the deposited molecule is about 2.70 eV ( $\beta_2 \approx 1, \beta_4 \approx 0$ ). A P<sub>4</sub> contribution to the anisotropy is observed peaking at 2.75 eV ( $\beta_4 \approx 0.5$ ). The latter feature is the signature of a non-resonant two photon process. It is also indicative of the real vertical Ionization Energy (IE) of the deposited DABCO. Indeed, the species symmetry of DABCO in its S<sub>1</sub> state is A', its single photon ionization leads to a P<sub>4</sub>-free signal. The main signal peak (S<sub>1</sub>-resonant ionization) contains some information on the relaxation of the intermediate S<sub>1</sub> levels, which will be described below. The deposited DABCO molecule shows a sharper band of 0.15 eV fwhm than the one of isolated DABCO measured under the same laser conditions. The anisotropy feature at P<sub>4</sub> shows a 0.10 eV fwhm, at the resolution limit of our detector. The vertical IE of the deposited DABCO is also measured at 6.60 ± 0.15 eV. This value is nearly 0.72 eV higher in energy than the one measured for the isolated molecule.<sup>17,19</sup> The IE difference is defined as the solvation energy difference between the neutral and the ion molecules, for the S<sub>0</sub> ground state geometry.

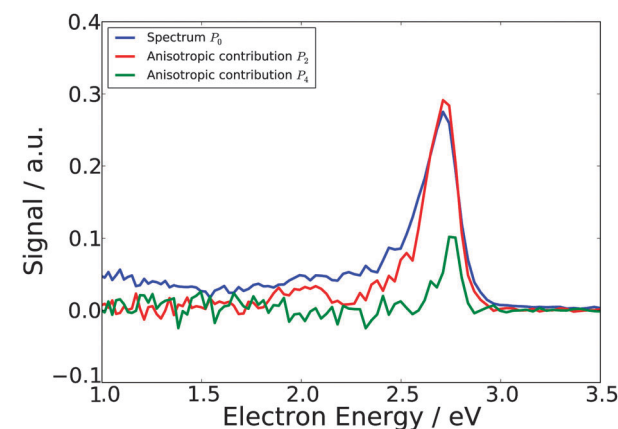


**Fig. 8** p-BASEX inverted photoelectron spectra. Ionization by two photons 265.1 nm (fwhm 2.12 nm) of deposited DABCO.

In a previous work on the TDMAE molecule, the IE difference was measured to be around 0.34 eV.<sup>11</sup> It seems here that the solvation of the ion is much stronger for the DABCO molecule than it was for TDMAE. This is probably because, in TDMAE, charges on the nitrogen atoms are shielded by the 8 methyl substituents, secluding the argon atoms and limiting the stabilization.

The asymmetric shape of the two photon photoelectron spectra confirms the preceding hypothesis of the existence of two sites in the ground state for the deposited cluster. At this energy (2.7 eV) resolution becomes insufficient to resolve the two photoelectron peaks originating from the ground state isomers.

## 6.2 Time-resolved dynamics: one photon probe

The time-resolved photoelectron signal is presented in Fig. 9 for a pump of 265.1 nm and a probe of 399 nm (3.10 eV); both having the same polarization (parallel to the detector). The initially populated state that we probe shows a peak at 0.88 eV having a smooth dynamics. Its intensity seems distributed over two outgoing channels: one remaining at the same energy, around 0.9 eV (Track 1, yellow), and the other one (Track 2) slightly lower in energy at 0 ps delay time and going down

smoothly in energy between 0 and 0.6 ps. Above 0.6 ps, Track 2 corresponds to photoelectrons with an energy of around 0.73 eV. Actually, upon careful analysis of Track 2 shows a non-Gaussian profile which can be decomposed into two Gaussian subtracks, having a constant energy gap between them (sub-tracks 2a and 2b as labeled in the figure). In the following, Track 2 refers to the sum of sub-tracks 2a and 2b. Note that Track 2a points at the maximum of the signal and will be considered when looking at the energy evolution, whereas Track 2 will be monitored when looking at signal intensities. The signal observed at about 0.38 eV is due to the isolated DABCO<sup>17</sup> (Track 3), and the signal at very low energy is attributed to an autoionization process of poor efficiency. The results which are presented here correspond to an average cluster size of 800 atoms. A similar study, which is not reported here, was performed on smaller clusters. It did not show any remarkable difference (except in the global intensity of the signal). Hence, no large effect of the cluster size, nor of the cluster size distribution is expected in observation reported here.

The signal shows definitely some peaks evolving in time. This evolution concerns the peak intensities, as usual for

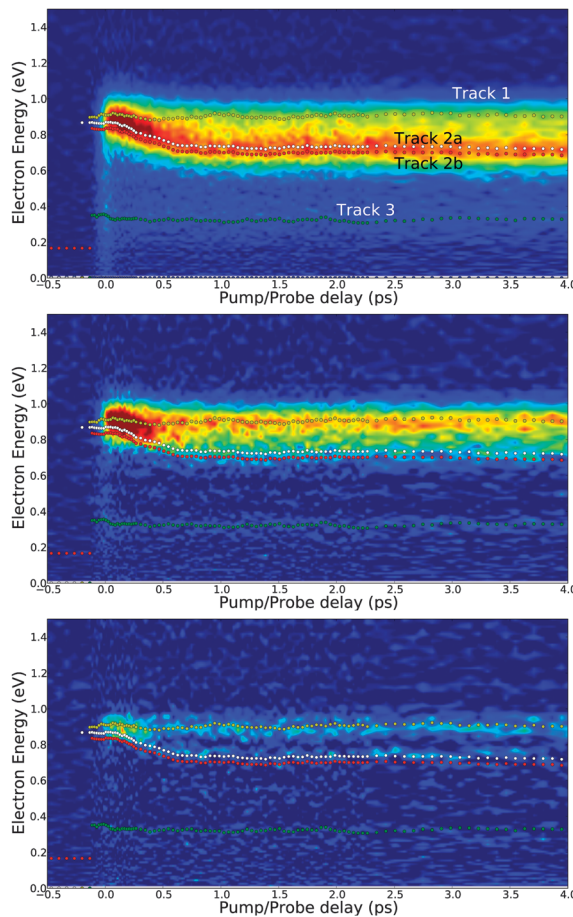


**Fig. 9** Time-resolved photoelectron signal for the 263 nm pump/392 nm probe, parallel polarization. The evolution is given for the whole signal  $P_0$  (top), the second order Legendre polynomial function  $P_2$  (middle), the forth order Legendre polynomial function  $P_4$  (bottom). The dots are the result of the track signal decomposition.

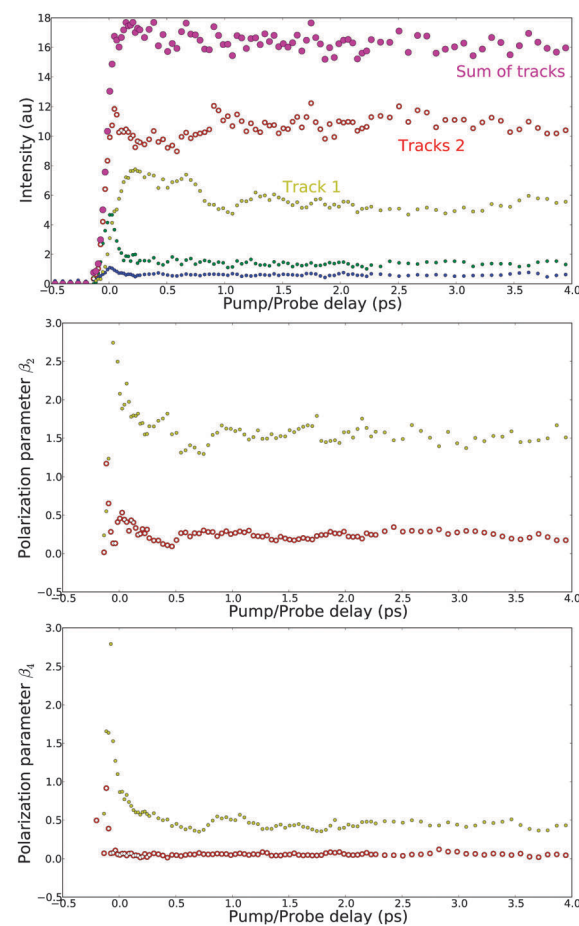


**Fig. 10** Time-resolved evolution of the intensity of tracks (top) and of their polarization parameters  $\beta_2$  and  $\beta_4$  for the 265 nm pump/399 nm probe, parallel polarization. The markers in all figures refer to the same tracks as in Fig. 9. The intensities of Tracks 2a & b are summed under the label Tracks 2. Magenta marker is the sum of Tracks 1 and 2.

molecular relaxation,<sup>17,51</sup> and also the central energy. Recently, we showed that the relaxation of barium deposited on an argon cluster<sup>13</sup> presents such behavior. Fitting the energy of Track 2 with an exponential decay gives a 270 fs relaxation time (see ESI†).

When looking at the sum of the intensities of the Tracks 1 and 2 (see Fig. 10-top), it appears that the total signal remains almost constant within the time scale displayed. The decomposed intensities show some fluctuations out of the noise attributed to the track decomposition procedure used. Indeed, at short times, the two main tracks are overlapping in energy and the relative signal distribution is undetermined, *i.e.* very sensitive to the experimental noise. Roughly we can consider that the intensity of the two tracks is constant within the first picosecond. This is not the case when looking at the P<sub>2</sub> component of the signal (see Fig. 9). Initially, as the main tracks are superimposed, the whole signal seems to be polarized whereas, at long time, only Track 1, higher in energy, remains strongly polarized  $\beta_2 \approx 1.5/\beta_4 \approx 0.4$  (*versus*  $\beta_2 \approx 0.3/\beta_4 \approx 0.0$  for Track 2). This points out the common origin of the two tracks: the same excited species on the cluster can lead to two different structures: one gives a polarized electron of 0.90 eV energy and the other results in a poorly polarized electron of 0.73 eV energy. Note that the intensity ratio between Tracks 1 and 2 is 1:2. Nevertheless, this ratio of intensities is affected by a strong rotational anisotropy which will be the object of a forthcoming paper.

Based on the shape of the S<sub>1</sub> potential described above for the DABCO··Ar<sub>3</sub> clusters, after population of the solvated DABCO cluster potential well in the Franck–Condon geometry (as for the D<sub>3h</sub> form of DABCO··Ar<sub>3</sub>), the distance between DABCO and argon increases. This solvation dynamics may destabilize the second shell which induces a larger dynamics. The probe photon promotes the wavepacket into the D<sub>0</sub> ionic potential. Since the long distance part of S<sub>1</sub> is flat, a “quite constant” photoelectron signal is rapidly recorded.

Looking at the relative energies between the ionic state and the excited states (see Tables 1 and 2) one can link the signal given by the nanosecond experiment and the femtosecond time resolved one, Peak 1 and Track 1 and, respectively, Peak 2 and Track 2. The difference in energy ( $\Delta E_i = E_{\text{Track}_i}(4 \text{ ps}) - E_{\text{Peak}_i}(4 \text{ ns})$ ) can be attributed to some inaccuracy in the measurement of the UV wavelength for the fs experiment and on the time delay between the pump and the probe: the final energy is not reached in so short a time.

As we discussed already, it appears clearly in Fig. 6 at 4.61 eV that there are two isomers present in the jet after deposition of the DABCO molecule on the argon cluster. These peaks are separated by 0.21 eV. The peak corresponding to the highest electron energy is the most solvated in S<sub>0</sub> (Peak 1). It is not

**Table 2** Photoelectron energies for a pump of 265.1 nm and a probe of 399 nm (3.13 eV)

	Energy at 4 ps (eV)	Energy below IE (eV)	fwhm (eV)
Track 1	0.90	-2.20	0.11
Track 2	0.73	-2.37	0.12

unfamiliar for large clusters such as the ones here to exhibit isomeric forms. The hydrated electron in water shows bands in the electron photo-detachment spectrum that can be readily identified as interior and exterior isomers,<sup>52</sup> to interior charges or surface charges. This stems from the pick-up deposition technique, which entrains the molecule at the surface of the cluster. The fact that it remains there is proved by the polarization of the ejected electrons which is rather high  $0.4 < \beta < 1.5$ ; this can only be the case if the electrons are ejected from the surface.

More interestingly, we observe that during the excited state solvation process, one species interconverts into the other one. We noticed indeed in Fig. 9 that the photoelectron signal resulting from the 265 nm (4.68 eV) excitation splits into Track 1 which evolves at constant energy into Peak 1 and another one, Track 2, at lower electron energies (by 0.17 eV), which evolves into Peak 2 after a further decay of the photoelectron energy. Since no electronic relaxation is expected from S<sub>1</sub>, even deposited on the cluster, we point to a reorganization process of the solvent shell during the time scale of the experiment, with a time constant of 270 fs for the first shell reorganization, which, given the number of atoms in the cluster is reasonable. This reorganisation might correspond to a reorientation of the DABCO molecule with its diffuse Rydberg orbital. In the S<sub>1</sub> state, these could tend to come away from the maximum number of atoms and the molecule rotates with respect to the argon surface, showing one of its side to the vacuum, and limiting also the number of argon in the first shell.

Comparing the ratio of isomeric peaks in Fig. 7 at 4.618 eV, we observe a ratio of about 1:1 in favor of the highest energy electron Peak 1 while it becomes 1:5 in favor of the less solvated one at 265 nm. Nevertheless, for an excitation at 265 nm, as seen already, the time resolved evolution shows an initial distribution mainly focused on the most solvated species. It splits later into Tracks 1 and 2 which converge, respectively, toward Peaks 1 and 2. Thus, with the excess energy released in the population of S<sub>1</sub> at 265 nm within the cluster, the best solvated isomer in S<sub>0</sub> interconverts partially (Track 2) into the other isomer in S<sub>1</sub>, as shown earlier. This appears also in the nanosecond experiments, keeping in mind that the ionization is a resonant [1 + 1] ionisation: S<sub>1</sub> is populated and a second photon  $\approx 266$  nm ionizes the molecule within the 5 ns pulse duration, *i.e.* after the interconversion or relaxation of the solvation has occurred. As seen above, at 265 nm the ratio between Peaks 1 and 2 is in rough agreement with the 4 ps ratios in femtosecond experiments. Hence the rise of the signal of Peak 2 above 268 nm to higher energies is not due to a higher absorption but to an interconversion of one isomer to the other in S<sub>1</sub>. This interconversion process likely starts at the top of Peak 1, *i.e.*  $\sim 23$  meV ( $\sim 185 \text{ cm}^{-1}$ ) above the S<sub>1</sub> absorption threshold, giving the minimal extra energy required for this process to happen. From  $\sim 40$  meV ( $\sim 320 \text{ cm}^{-1}$ ) above the S<sub>1</sub> absorption threshold, most of the species available for an interconversion seems to be affected since the intensity of Peak 2 reaches a plateau. Nevertheless, the ratio between both bands gradually increases, signature of the continuous rise of the interconversion process with the absorption.

Finally, as expected from the REMPI-PES analysis, no track is observed, which would correspond to probing ejected DABCO molecules. This is actually not surprising since the excess energy provided by the excitation is not large enough to induce ejection, whereas it is enough to drive the interconversion process.

### 6.3 Time-resolved dynamics: two photon probe

Multiphoton ionization is a complementary technique to one-photon ionization for the characterization of dynamics.<sup>17</sup> Indeed, it takes advantage from intermediate resonances to enhance selectively the ionization for some well defined geometries, emphasising some changes that would not be visible otherwise. Fig. 11 shows the time resolved dynamics of the DABCO $\cdot\cdot\cdot$ Ar<sub>n</sub> cluster system, excited at 265 nm and probed at 792 nm. The same general relaxation dynamics appears clearly. In addition, after a short relaxation, the evolution appears to be more like a jump from one geometry to another one. It looks like an intermediate resonance in the intermediate states reached by the 792 nm photons, has disappeared as the interaction of DABCO with its environment has been modified through its evolution in S<sub>1</sub>. When looking more carefully,

especially at the P<sub>4</sub> component, another jump appears also at very short time delays. These jumps are supported by the MRCI calculations of DABCO $\cdot\cdot\cdot$ Ar<sub>n</sub> (small n),<sup>29</sup> which show non-parallel evolutions of the Rydberg state energies as a function of the DABCO $\cdot\cdot\cdot$ Ar distance. S<sub>1</sub>, S<sub>2</sub>, S<sub>3</sub> and S<sub>4</sub> having a different behaviour with the argon distance, the resonances are localized at a specific geometry of the potential energy surface, hence at a specific time as the system proceeds to relax. Note that these various evolutions are understood by the different s and p Rydberg character of the excited states. As a consequence, the transition moments computed for the DABCO $\cdot\cdot\cdot$ Ar<sub>n</sub> (small n) clusters are large for the S<sub>p'</sub> ( $p' \geq 1$ )  $\leftarrow$  S<sub>p</sub> ( $p' \geq 1$ ) transitions (see ESI†), in line with the ionization enhancements as the probe energy matches the transition energy. However it remains impossible at the current state-of-the-art of calculation to attribute the accurate geometry of the resonance.

In terms of electron polarization, the lower energy electrons ( $\sim 0.7$  eV) show a much stronger P<sub>2</sub> polarization than for the one-photon probe and the high energy electrons show a much stronger P<sub>4</sub> polarization with respect to the single-photon probe. The addition of an intermediate state in the ionization process is compatible with these increases in polarization, since a new transition momentum is involved in the transition.

## 7 Conclusion

In the present paper we scrutinised the relaxation dynamics of an electronically excited molecule in a Rydberg state in the presence of a chemically inert medium. This joint theoretical and experimental investigation has been focussed on the DABCO molecule deposited upon an argon cluster.

Two solvation sites on the cluster were observed spectroscopically, differing through an absorption threshold of  $60\text{ cm}^{-1}$  and a photoelectron energy of 0.21 eV. Photoelectron energies, electron polarisations of the absorption spectra, all observations indicate that the excited state converts one site into another (see Fig. 12). This is a rare example of such observations and it could be possibly ascribed to a reorientation of the Rugby shaped DABCO molecule at the surface of the cluster. We will investigate further with time dependent cross

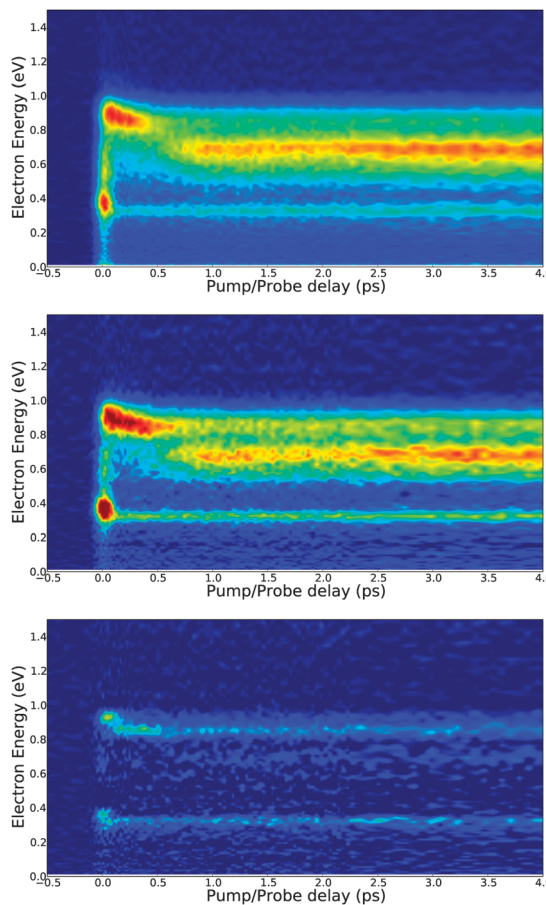


Fig. 11 Time resolved photoelectron signal for the 265 nm pump/792 nm probe, parallel polarization. The evolution is given for the whole signal P<sub>0</sub> (top), the second order Legendre polynomial function P<sub>2</sub> (middle), the forth order Legendre polynomial function P<sub>4</sub> (bottom).

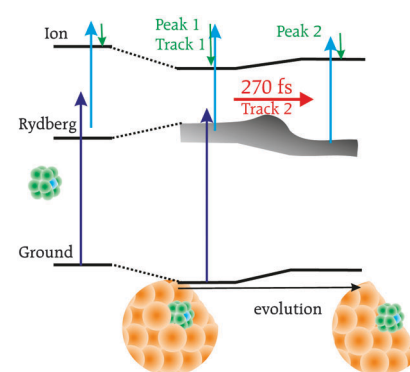


Fig. 12 Schematic structure and energy of the deposited DABCO molecules on the argon cluster. Structures are purely speculative.

polarisation effects this phenomenon. We wish specially to characterise better the position of the DABCO molecule with respect to the surface. All indications show that the molecule is close to the surface (electron polarisation). We have also observed that in the first Rydberg state, the repulsive interaction with the inert solvent dominates and the argon atoms have not made their way to the ionic core.

A dynamics of 270 fs was measured for the change in the solvation environment from the more solvated one to the less solvated one, which appears to be the more stable one in the excited state. The height of the barrier was measured at  $\sim 185 \text{ cm}^{-1}$ . At an energy of  $320 \text{ cm}^{-1}$  above the absorption threshold, about 85–70% of the excitation induces a solvation dynamics. The remaining 15–30% of deposited molecules having no dynamics.

It appears in this paper that such studies are of strong interest for the relaxation dynamics of the electronically excited molecules deposited at an interface. Since the interaction with a medium is strongly dependent on the state populated, the molecules adapt to their neighborhood as a function of the electronic state reached by the photons, the higher electronic state or even ionic states.

Through this work, several important issues can be drawn on the ultrafast relaxation dynamics of molecules deposited at interfaces (liquid–gas). This work fills the gap between pure gas phase studies<sup>17,31,36</sup> and those performed in matrices.<sup>2,3,7–9</sup>

## Acknowledgements

S.A. thanks EU-ITN project ICONIC-238671 for funding. L.P. thanks the ANR for support through the contract ANR-09-JCJC-0090-01 CHROMADYNE. Furthermore, we thank the CEA/SLIC staff, in particular Olivier Gobert and Michel Perdris, for technical support.

## References

- B. Katz, M. Brith, A. Ron, B. Sharf and J. Jortner, *Chem. Phys. Lett.*, 1968, **2**, 189–193.
- M. Chergui, N. Schwentner and W. Bohmer, *J. Chem. Phys.*, 1986, **85**, 2472–2482.
- M. Chergui, N. Schwentner and V. Chandrasekharan, *J. Chem. Phys.*, 1988, **89**, 1277–1284.
- F. Vigliotti and M. Chergui, *Eur. Phys. J. D*, 2000, **10**, 379–390.
- M. Ben El Hadj Rhouma, Z. Ben Lakhdar, H. Berriche and F. Spiegelman, *J. Chem. Phys.*, 2006, **125**, 084315.
- F. Ben Salem, M. Ben El Hadj Rhouma, F. Spiegelman, J. M. Mestdagh and M. Hochlaf, *J. Chem. Phys.*, 2012, **137**, 224310.
- C. Jeannin, M. T. Porrella-Oberli, S. Jimenez, F. Vigliotti, B. Lang and M. Chergui, *Chem. Phys. Lett.*, 2000, **316**, 51–59.
- G. Rojas-Lorenzo, J. Rubayo-Soneira, F. Vigliotti and M. Chergui, *Phys. Rev. B: Condens. Matter Mater. Phys.*, 2003, **67**, 115119.
- F. Vigliotti, L. Bonacina, M. Chergui, G. Rojas-Lorenzo and J. Rubayo-Soneira, *Chem. Phys. Lett.*, 2002, **362**, 31–38.
- M. C. Duval, O. B. Dazy, W. H. Breckenridge, C. Jouvet and B. Soep, *J. Chem. Phys.*, 1986, **85**, 6324–6334.
- L. Poisson, E. Gloaguen, J.-M. Mestdagh, B. Soep, A. Gonzalez and M. Chergui, *J. Phys. Chem. A*, 2008, **112**, 9200–9210.
- M. C. Heitz, L. Teixidor, N. T. Van-Oanh and F. Spiegelman, *J. Phys. Chem. A*, 2010, **114**, 3287–3296.
- A. Masson, L. Poisson, M. A. Gaveau, B. Soep, J. M. Mestdagh, V. Mazet and F. Spiegelman, *J. Chem. Phys.*, 2010, **133**, 054307.
- Q. Y. Shang and E. R. Bernstein, *Chem. Rev.*, 1994, **94**, 2015–2025.
- A. M. Halpern, J. L. Roebber and K. Weiss, *J. Chem. Phys.*, 1968, **49**, 1348–1357.
- D. H. Parker and P. Avouris, *Chem. Phys. Lett.*, 1978, **53**, 515–520.
- L. Poisson, R. Maksimenska, B. Soep, J. M. Mestdagh, D. H. Parker, M. Nsangou and M. Hochlaf, *J. Phys. Chem. A*, 2010, **114**, 3313–3319.
- E. Heilbronner and K. A. Muszkat, *J. Am. Chem. Soc.*, 1970, **92**, 3818–3821.
- M. J. Watkins and M. C. R. Cockett, *J. Chem. Phys.*, 2000, **113**, 10560–10571.
- D. Consalvo, J. Oomens, D. H. Parker and J. Reuss, *Chem. Phys.*, 1992, **163**, 223–239.
- D. H. Parker and P. Avouris, *J. Chem. Phys.*, 1979, **71**, 1241–1246.
- M. A. Quesada, Z. W. Wang and D. H. Parker, *J. Phys. Chem.*, 1986, **90**, 219–222.
- V. Galasso, *Chem. Phys.*, 1997, **215**, 183–190.
- D. E. Belcher, M. J. Watkins, N. Tonge and M. C. R. Cockett, *J. Chem. Phys.*, 2004, **120**, 7894–7900.
- Q. Y. Shang, P. O. Moreno, S. Li and E. R. Bernstein, *J. Chem. Phys.*, 1993, **98**, 1876–1887.
- G. Vandenhoeck, D. Consalvo, D. H. Parker and J. Reuss, *Z. Phys. D: At., Mol. Clusters*, 1993, **27**, 73–78.
- Q. Y. Shang, P. O. Moreno and E. R. Bernstein, *J. Am. Chem. Soc.*, 1994, **116**, 311–319.
- K. Mathivon, R. Linguerri and M. Hochlaf, 2013, submitted.
- K. Mathivon, R. Linguerri and M. Hochlaf, 2013, submitted.
- S. Soorkia, N. Shafizadeh, J. Lievin, M.-A. Gaveau, C. Pothier, J.-M. Mestdagh, B. Soep and R. W. Field, *J. Phys. Chem. A*, 2011, **115**, 9620–9632.
- L. Poisson, K. D. Raffael, B. Soep, J. M. Mestdagh and G. Buntinx, *J. Am. Chem. Soc.*, 2006, **128**, 3169–3178.
- L. Poisson, K. D. Raffael, M. A. Gaveau, B. Soep, J. M. Mestdagh, J. Caillat, R. Taieb and A. Maquet, *Phys. Rev. Lett.*, 2007, **99**, 103401.
- L. Poisson, P. Roubin, S. Coussan, B. Soep and J. M. Mestdagh, *J. Am. Chem. Soc.*, 2008, **130**, 2974–2983.
- J. M. Mestdagh, M. A. Gaveau, C. Gee, O. Sublemontier and J. P. Visticot, *Int. Rev. Phys. Chem.*, 1997, **16**, 215–247.
- A. Eppink and D. H. Parker, *Rev. Sci. Instrum.*, 1997, **68**, 3477–3484.
- A. Stolow, A. E. Bragg and D. M. Neumark, *Chem. Rev.*, 2004, **104**, 1719–1757.

- 37 A. V. Baklanov, L. M. C. Janssen, D. H. Parker, L. Poisson, B. Soep, J.-M. Mestdagh and O. Gobert, *J. Chem. Phys.*, 2008, **129**, 214306.
- 38 G. A. Garcia, L. Nahon and I. Powis, *Rev. Sci. Instrum.*, 2004, **75**, 4989–4996.
- 39 L. Poisson, *LV\_pBASEX*, 2009.
- 40 S. Sorgues, J. M. Mestdagh, J. P. Visticot and B. Soep, *Phys. Rev. Lett.*, 2003, **91**, 103001.
- 41 C. Ruckebusch and L. Blanchet, *Anal. Chim. Acta*, 2013, **765**, 28–36.
- 42 V. Mazet, S. Faisan, A. Masson, M. A. Gaveau, L. Poisson and J. M. Mestdagh, *IEEE Workshop on Statistical Signal Processing*, August 2012, Ann Arbor, USA, pp. 253–256.
- 43 V. Mazet, S. Faisan, S. Awali, M. A. Gaveau and L. Poisson, *IEEE Trans. Signal Process.*, 2013, submitted.
- 44 S. G. Razul, W. J. Fitzgerald and C. Andrieu, *Nucl. Instrum. Methods Phys. Res., Sect. A*, 2003, **497**, 492–510.
- 45 V. Mazet, *IEEE Signal Process. Lett.*, 2011, **18**, 181–184.
- 46 P. J. Green, *Biometrika*, 1995, **82**, 711–732.
- 47 F. M. Tao and Y. K. Pan, *Mol. Phys.*, 1994, **81**, 507–518.
- 48 K. Patkowski, G. Murdachaew, C. M. Fou and K. Szalewicz, *Mol. Phys.*, 2005, **103**, 2031–2045.
- 49 Q. Y. Shang, P. O. Moreno, C. Dion and E. R. Bernstein, *J. Chem. Phys.*, 1993, **98**, 6769–6778.
- 50 N. H. Nahler, M. Farnik, U. Buck, H. Vach and R. B. Gerber, *J. Chem. Phys.*, 2004, **121**, 1293–1302.
- 51 E. Gloaguen, J. M. Mestdagh, L. Poisson, F. Lepetit, J. P. Visticot, B. Soep, M. Coriou, A. T. J. B. Eppink and D. H. Parker, *J. Am. Chem. Soc.*, 2005, **127**, 16529–16534.
- 52 J. R. R. Verlet, A. E. Bragg, A. Kammerath, O. Cheshnovsky and D. M. Neumark, *Science*, 2005, **307**, 93–96.